Sensors and Actuators A 209 (2014) 183–190

Contents lists available at ScienceDirect

Sensors and Actuators A: Physical

journal homepage: www.elsevier.com/locate/sna

A high electromechanical coupling coefficient SH0 Lamb wave lithium niobate micromechanical resonator and a method for fabrication

Roy H. Olsson III[a,*], Khalid Hattar[b], Sara J. Homeijer[c], Michael Wiwi[c], Matthew Eichenfield[a], Darren W. Branch[d], Michael S. Baker[a], Janet Nguyen[a], Blythe Clark[b], Todd Bauer[c], Thomas A. Friedmann[c]

[a] MEMS Technologies Department, Sandia National Laboratories, United States
[b] Radiation-Solid Interactions Department, Sandia National Laboratories, United States
[c] MESAFAB Operations Department, Sandia National Laboratories, United States
[d] Biosensors and Nanomaterials Department, Sandia National Laboratories, United States

ARTICLE INFO

Article history:
Received 5 November 2013
Received in revised form 17 January 2014
Accepted 22 January 2014
Available online 30 January 2014

Keywords:
Contour mode resonator
Coupling coefficient
Lamb wave resonator
Lithium niobate
Microresonator

ABSTRACT

We present a high coupling coefficient, k^2_{eff}, micromechanical resonator based on the propagation of SH0 Lamb waves in thin, suspended plates of single crystal X-cut lithium niobate ($LiNbO_3$). The thin plates are fabricated using ion implantation of He to create a damaged layer of $LiNbO_3$ below the wafer surface. This damaged layer is selectively wet etched in a hydrofluoric (HF) acid based chemistry to form thin, suspended plates of $LiNbO_3$ without the wafer bonding, layer fracturing and chemical mechanical polishing in previously reported $LiNbO_3$ microfabrication approaches. The highest coupling coefficient is found for resonators with acoustic propagation rotated 170° from the *y*-axis, where a fundamental mode SH0 Lamb wave resonator with a plate width of 20 μm and a corresponding resonant frequency of 101 MHz achieves a k^2_{eff} of 12.4%, a quality factor of 1300 and a resonator figure of merit (*M*) of 185. The k^2_{eff} and *M* are among the highest reported for micromechanical resonators.

1. Introduction

Microresonators are miniature acoustic resonators fabricated using integrated circuit (IC) microfabrication techniques. Microresonators are of great interest since the CAD-definable resonant frequency allows many filters spanning from several hundred MHz to several GHz to be realized on a single chip [1,2]. This is especially important for next generation cellular handsets where the growing number of frequency bands each typically require a discrete filter die. Microresonator technology provides a potential path for integrating many band select filters on a single die, thus reducing the size, cost and complexity of next generation wireless handsets.

Currently band select filters in cellular handsets are realized using a combination of many dies containing bulk [3–5] (BAW) or surface [3,4,6,7] (SAW) acoustic wave resonators. Aluminum nitride (AlN) based BAW resonators and SAW resonators formed in lithium niobate ($LiNbO_3$) or lithium tantalate ($LiTaO_3$) have the high coupling coefficients, k^2_{eff}, required to achieve the required band select filter bandwidths of ~3% of the filter center frequency and the quality factors required for steep filter roll off all while maintaining low filter insertion loss. AlN BAW resonators operate with frequencies defined by the thickness of a deposited thin film and require a separate film thickness for each filter frequency. This dependency on film thickness makes integration of multiple frequency filters on a single die both challenging and costly. While in theory SAW resonators can support a wide range of frequencies on a single chip, in practice, the thickness of the metal interdigitated electrodes used to transduce SAW resonators is varied with frequency [7], limiting the range of filter bands that can be covered on a single chip. Furthermore, the low SAW phase velocity limits the application of SAW technology in emerging high frequency bands above 2.5 GHz [3].

Recently, both piezoelectric [1,8–12] and electrostatically [2,13,14] transduced microresonators have been the subject of research. By establishing the resonance from a laterally propagating Lamb wave in a suspended plate with a thickness less than an acoustic wavelength, a wide range of filter frequencies can be achieved on a single wafer by altering the CAD-layout of the devices. The k^2_{eff} of electrostatically driven resonators [15] at frequencies relevant to cellular communications are orders of magnitude lower than that required for band select filters. Piezoelectric Lamb wave resonators formed in deposited thin films of aluminum nitride (AlN), zinc oxide (ZnO) and lead zirconate titanate (PZT), while having much higher coupling coefficients than electrostatically

* Corresponding author. Tel.: +1 505 284 6375.
E-mail address: rholsso@sandia.gov (R.H. Olsson III).

0924-4247/$ – see front matter © 2014 Elsevier B.V. All rights reserved.
http://dx.doi.org/10.1016/j.sna.2014.01.033

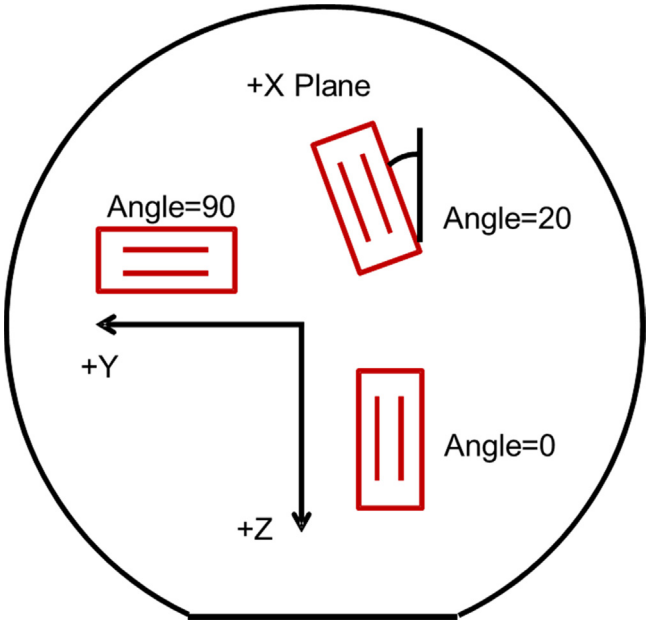

Fig. 1. Top down schematic of an X-cut $LiNbO_3$ wafer showing the *z* and *y* crystal planes. The coupling coefficient and sound velocity for each Lamb mode vary with the direction of acoustic propagation.

transduced microresonators, still do not have a high enough coupling coefficient for many of the band select filters in wireless handsets.

In 2001 Kuznetsova et al. [16] reported the theoretically large piezoelectric coupling that could be achieved for Lamb resonators in thin films of single crystal $LiNbO_3$. The largest coupling reported in [16] was for the SH0 Lamb mode in X-cut $LiNbO_3$ with a k^2_{eff} of 27.4%. The challenge is in realizing thin, suspended membranes of single crystal piezoelectric materials with much higher coupling coefficients than the deposited polycrystalline piezoelectric thin films such as AlN, ZnO and PZT. Recently, symmetric (S0) Lamb wave microresonators have been reported in suspended thin films of single crystal X-cut [15] and 136° rotated Y-cut [17] $LiNbO_3$. Both of the fabrication processes reported in [15,17] require bonding of a $LiNbO_3$ device wafer to a handle wafer using a glue layer. Thin films of $LiNbO_3$ directly over the glue/release layer are then realized either by polishing back the $LiNbO_3$ device wafer to the desired thickness of ~1 μm [17] or by fracturing the $LiNbO_3$ device wafer [15,18,19] just below the wafer surface that was previously ion implanted to induce a damaged fracture plane.

In this paper, we report a Lamb wave $LiNbO_3$ microresonator fabricated in a process similar to that reported in [20,21] that does not require costly wafer bonding, fracturing or polishing processes. The thin plates are fabricated using ion implantation of He to create an ion damaged layer of $LiNbO_3$ at a desired depth below the wafer surface. This damaged layer is selectively wet etched in a hydrofluoric (HF) acid based chemistry to form thin, suspended plates of $LiNbO_3$. Using this fabrication process we report high coupling coefficient SH0 Lamb wave resonators in X-cut $LiNbO_3$. The highest coupling coefficient is found for resonators with acoustic propagation rotated 170° from the *y*-axis (see Fig. 1); a rotation which is in agreement with the theory reported in [16]. A fundamental mode SH0 Lamb wave resonator propagating in a ~1.2 μm thick plate with a width of 20 μm and a corresponding resonant frequency of 101 MHz achieves a measured k^2_{eff} of 12.4%, a quality factor of 1300 and a resonator figure of merit (*M*) of 185. The k^2_{eff} and M are among the highest measured for micromechanical resonators [15].

Table 1
Etch rates of the damaged release layer and the different faces of the $LiNbO_3$ crystal in the hydrofluoric acid release chemistry.

Crystal face	Ion damaged release layer	+*x*, −*x*	+*y*, −*y*	+*z*	−*z*
Etch rate (nm/h)	9000	14	204	<14	2200

2. Single crystal lithium niobate microfabrication process

The $LiNbO_3$ microresonators are fabricated using the process flow shown in Fig. 2. (A) The process begins with the evaporation of 100 nm of Cr and the patterning of alignment marks in the Cr on X-cut $LiNbO_3$. (B) Next, an oxide layer is deposited and patterned to define where an ion implant will penetrate the $LiNbO_3$ creating an ion damaged $LiNbO_3$ release layer at the end of the ion implant range. Patterning where the ion implant penetrates the $LiNbO_3$ allows the lateral extents of the device release to be precisely controlled. The sample is then implanted with a He dose of 1×10^{16} atoms/cm^3 at an energy of 0.8 MeV to create an ion damaged release layer of $LiNbO_3$ approximately 1.8 μm below the wafer surface. The implants are performed in a 3 MV NEC Pelletron using a current of <7 μA. To maintain a low sample temperature, the $LiNbO_3$ is cooled by liquid nitrogen using a Cu braid during implantation. While the ion implant passes through the Cr electrodes in the device region, measurements confirm that the Cr resistivity is not altered by the ion implant. (C) Then trenches that define the final resonator dimensions and resonant frequency are etched in the $LiNbO_3$ exposing the ion damaged $LiNbO_3$ release layer. The $LiNbO_3$ is dry etched at 15 °C using an $Ar/BCl_3/Cl_2$ gas mixture at 10 mT on a PlasmaTherm Versaline 4 in. ICP system using a newly optimized process. This process is capable of producing sidewalls with >80° sidewall angle and etch depths >2 μm. (D) Next, the Cr electrodes are patterned. (E) Optionally, a 1 μm Au layer is deposited and patterned to protect the −*z* face of the $LiNbO_3$ during the release. During our research we measured the etch rates in our wet hydrofluoric acid release chemistry for the ion damaged $LiNbO_3$ and for the different crystal faces of $LiNbO_3$. These etch rates are shown in Table 1. Additional studies of etching $LiNbO_3$ in aqueous HF can be in found in [22,23]. While the etch rates of the +*z*, *y* and *x* crystal faces are much lower than the ion damaged $LiNbO_3$, the etch rate of the −*z* face is only 4 times lower than that of the ion damaged $LiNbO_3$. Since the highest k^2_{eff} microresonators rotated 170° from the *y*-axis have a slight −*z* face component for one of the resonator sidewalls, this Au layer is used to protect the −*z* face and more accurately control the final dimensions of the microresonator. (F) The device is released using a wet hydrofluoric acid chemistry to remove the ion end of range damage in the $LiNbO_3$ and the devices are annealed at >300 °C to heal the implant damage in the device layer and flatten the devices. Finally, if utilized, the Au layer used to protect the −*z* face of the microresonator sidewall is stripped in a mixture of potassium iodide and iodine, $KI\text{-}I_2$.

A scanning electron micrograph (SEM) image of a $LiNbO_3$ microresonator with acoustic propagation rotated 170° from the *y*-axis is shown in Fig. 3. The designed microresonator dimensions are for a width, $W = 20$ μm, length, $L = 140$ μm and an electrode overlap, $a = 50$ μm. Each Cr electrode is 5 μm wide and the gap between electrodes is also 5 μm. The acoustic wave propagates in the width extensional direction, i.e. the direction of *W*. A zoomed in image of a suspended $LiNbO_3$ microresonator is shown in Fig. 4. Addition SEM images (not shown) of the underside of the $LiNbO_3$ resonators reveal a smooth surface and a final plate thickness of approximately 1.2 μm. Fig. 5 shows an optical image of a $LiNbO_3$ microresonator with acoustic propagation rotated 160° from the *y*-axis just prior to release. The device in Fig. 5 has the Au layer from Fig. 2(E) to protect the −*z* face of the microresonator during the HF